Molecular Vision 2024; 30:137-149 <http://www.molvis.org/molvis/v30/137>
Received 5 August 2023 | Accepted 18 March 2024 | Published 20 March 2024

The effect of age on aqueous humor of humans with high myopia

Kai Wen,[1] Mengjun Fu,[2] Yongtao Li,[1] Haorun Zhang,[2] Xiu Wang,[1] Yang Cai,[1] Yaoling Li,[1] Ruihong Su,[1] Yifang Huang,[1] Ming Liu,[1] Yufeng Zhang,[1] Shaozhen Zhao,[1] Jing Sun[1]

[1]Tianjin Key Laboratory of Retinal Functions and Diseases, Tianjin Branch of National Clinical Research Center for Ocular Disease, Eye Institute and School of Optometry, Tianjin Medical University Eye Hospital; [2]Weifang Eye Hospital, Shandong Province

Background: High myopia is a common cause of vision loss. Age is an important factor in the development of high myopia. However, the effect of age on aqueous humor proteins in the context of high myopia is unknown. This study explored the effect of age on the aqueous humor protein of humans with high myopia.
Methods: The aqueous humor of high myopia patients of different ages with implantable collamer lens implantation (ICL) was collected. Data-independent acquisition proteomic analysis was employed to explore differentially expressed proteins (DEPs). Two different bioinformatics analysis methods were used to interpret the proteomic results. Furthermore, three proteins were confirmed by enzyme-linked immunosorbent assay (ELISA).
Results: The study showed 18 upregulated and 20 downregulated proteins. The Kyoto Encyclopedia of Genes and Genomes (KEGG) analysis showed that the upregulated DEPs were highly enriched in coagulation and complement cascades. Weighted gene coexpression network analysis showed that the blue module was identified as a key module for high myopia and that the plasminogen (PLG) protein is a hub protein. ELISA confirmed that the expression levels of Alpha-1-antitrypsin were significantly upregulated in the aqueous humor of older patients presenting with high myopia.
Conclusions: This is the first study to investigate the effect of age on the level of aqueous humor protein in high myopia. Our study provided a comprehensive data set on the overall protein changes of different ages of human high myopia, shedding light on its potential molecular mechanism in high myopia damage to the eyeball.

It is well known that the incidence of high myopia is rapidly increasing worldwide. Currently, 2.7% of the world's population has high myopia, and this number will reach nearly 1 billion people by 2050 [1]. High myopia has a high risk of developing various ocular diseases and irreversible pathological damage to the eyeball. Ophthalmologists and researchers have arduously explored the pathogenesis of high myopia from multiple levels, including protein, RNA, and DNA. Some scholars believe that the level of oxidative stress in the eyeball may be related to the pathogenesis of high myopia in its correlation to damaging lipids, proteins, RNA, and DNA; promoting the expression of inflammatory factors; and causing cell death [2-5]. However, the specific mechanism of pathological damage in eyes with high myopia is unclear.

Aqueous humor and anterior lens capsule are commonly used clinical samples to explore eye diseases, including high myopia. Aqueous humor is continually produced by the ciliary body and is in direct contact with the anterior surface of the lens, iris, and corneal endothelial cells before draining out of the eye via the trabecular meshwork [6,7]. The chemical composition of aqueous humor depends not only on the naturally occurring components, but also on the metabolic exchange products of the tissues in the eye. Eye diseases can cause changes in the composition of the aqueous humor, especially the type and content of protein. Our previous studies showed that 58 differentially expressed proteins (DEPs, 211 proteins) in the aqueous humor of patients with high myopia, with the upregulated DEPs were highly concentrated in the coagulation and complement cascade [8]. The results of bioinformatics analysis showed that PLG and Kininogen-1 (KNG-1) may be pathogenic proteins of high myopia complicated by posterior scleral staphyloma [8]. The lens capsule, which is produced by the secretion of the lens epithelium, is a transparent and elastic membrane with uneven thickness that surrounds the lens. Our previous studies showed that the methyltransferase METTL14 and mRNA CHI3L1 m^6A modification levels in the anterior lens capsules of patients with high myopia were significantly upregulated [9]. All these findings indicate that the upregulation of methylase (METTL14) catalyzes the hypermethylation of gene CHI3L1, which may affect the expression level of its encoded protein YKL-40 and promote the remodeling of scleral tissue and change of the anatomic structure of the fundus of high myopia by participating in the process of PLG activation into plasmin and then regulating the composition of the extracellular matrix. However, there are some problems here: (1) the patients selected in the iTRAQ-based proteomic

Correspondence to: Jing Sun, No. 251, Fukang Road, Nankai District, Tianjin, 300110, Phone:86-18602668105, email: TMUeye@163.com

analysis of the aqueous humor were over 60 years old. High myopia caused changes in the anatomic structure of the fundus (posterior scleral staphyloma). In young patients with high myopia with no posterior scleral staphyloma, are the changes in protein—especially PLG and KNG-1 protein—consistent with previous studies? (2) Are there differences in the aqueous humor of patients with high myopia of different ages? (3) Is the expression of PLG protein related to age?

In the present study, we performed a specific variant of data-independent acquisition (DIA) proteomic analysis of the aqueous humor of patients of different ages with implantable collamer lens (ICL) implantation to identify changes in proteins. An enzyme-linked immunosorbent assay (ELISA) was performed to confirm the DIA results. Additionally, we used weighted gene coexpression network analysis (WGCNA) to identify age-related hub proteins. Our findings enhance our understanding of the mechanisms of high myopia damage to the eyeball in humans.

METHODS

Aqueous humor samples: In the current prospective study, 21 patients with high myopia who underwent uneventful implantation of a posterior-chamber phakic lens ICL at Tianjin Medical University Eye Hospital (Tianjin, China) were recruited, and their aqueous humor samples were collected during surgery. The inclusion criteria were as follows: (1) age ≥18 years; (2) stable refractive error (≤0.50 D change per year in refractive error in the past 2 years); (3) axis length ≥26 mm; (4) minimum anterior chamber depth (measured from the endothelium) 2.8 mm and minimum endothelial cell density 2500 cells/mm^2. The exclusion criteria were as follows: (1) other pre-existing ocular diseases; (2) suspicion of keratectasia; (3) history of ocular trauma or surgery; (4) systemic diseases, such as hyperthyroidism, autoimmune diseases, hypertension, diabetes, coronary heart disease, or severe mental disorders, such as anxiety and depression. Twenty-six aqueous humor samples of 21 patients of different ages, including 13 samples from each group, were selected . The aqueous humor of young patients with high myopia is abbreviated as “HM-recent” (patients with high myopia for less than 5 years), and the aqueous humor of older patients with high myopia is abbreviated as “HM-long-term” (patients with high myopia for more than 5 years). Table 1 shows the patient characteristics. The study was approved by the Human Research Ethics Committee of Tianjin Medical University Eye Hospital and adhered to the tenets of the Helsinki Declaration of 1975, as revised in 2000. Informed consent was obtained from all patients. All samples were collected into a cryopreservation tube and stored at −80 °C until use.

Sample preparation and fractionation for data dependent acquisition (DDA) library generation and DDA mass spectrometry assay: The amount of aqueous humor we took from each sample was about 0.25 ml. The protein concentration in aqueous humor was 0.23 mg/ml. Aqueous humor pools were separated from the most abundant proteins using Agilent Human 14 by following the manufacturer’s protocol (Agilent Technologies). The high- and low-abundance proteins were collected, respectively, and, the 10 kDa ultrafiltration tube (Sartorius) was used for desalination and concentration of high- and low-abundance components. One volume of sodium dodecyl sulfate (SDT, SDS; Dithiothreitol, DTT; TRIS hydrochloride, Tris-HCl) buffer (4% SDS, 100 mM DTT, 150 mM Tris-HCl pH 8.0) was added, boiled for 15 min, and centrifuged at 14,000 × *g* for 20 min. The supernatant was quantified with the BCA (bicinchoninic acid) Protein Assay Kit (Bio-Rad). The sample was stored at −80 °C. Filter-aided sample preparation was performed according to the filter-aided sample preparation(FASP) procedure [10]. All fractions for DDA library generation were injected on a Thermo Scientific Q Exactive HF X mass spectrometer connected to an Easy nLC 1200 chromatography system (Thermo Scientific) according to a previously published article [11].

Mass spectrometry assay for data-independent acquisition (DIA): Each sample peptide was analyzed by LC-MS/MS operating in the DIA mode by Shanghai Applied Protein Technology Co., Ltd. Each DIA cycle contained one full MS–SIM scan, and 30 DIA scans covered a mass range of 350–1800 m/z. Runtime was 90 min with a linear gradient of buffer B (80% acetonitrile and 0.1% formic acid) at a flow rate of 250 nl/min. Quality control (QC) samples (pooled sample from equal aliquot of each sample in the experiment) were injected with DIA mode at the beginning of the MS study and after every six injections throughout the experiment, which was used to monitor the MS performance.

Mass spectrometry data analysis: For the DDA library data, the FASTA sequence database was searched with SpectronautTM 14.4.200727.47784 software. The database was the UniProt human database, and the iRT peptides sequence was added (Biognosys|iRTKit|). The parameters were set as follows: enzyme is trypsin, max missed cleavages are 2, fixed modification is carbamidomethyl (C), and dynamic modification is oxidation (M) and acetyl (Protein N-term). All reported data were based on 99% confidence for protein identification as determined by false discovery rate (FDR=N(decoy)*2/(N(decoy)+ N(target))) ≤1%. A spectral library was constructed by importing the original raw files and DDA searching results into Spectronaut Pulsar X TM_12.0.20491.4 (Biognosys).

Table 1. Patient characteristics.

Samples	Gender	Ages	Duration of the disease	Axial(mm)	Degree of myopia(D)	Eye
HM-long-term						
	F	44	11y	26.92	−9.75	OD
	F	44	11y	27.71	−10.0	OS
	M	33	7y	26.73	−7.0	OS
	F	47	10y	29.95	−12.0	OD
	F	47	10y	31.24	−15.5	OS
	M	31	6y	26.64	−6.75	OD
	M	31	6y	26.74	−7.0	OS
	M	37	8y	26.14	−6.75	OS
	F	32	6y	26.24	−9.0	OD
	F	32	6y	26.59	−9.25	OS
	F	41	8y	28.77	−10.75	OS
	F	32	10y	27.61	−11.5	OS
	M	42	10y	27.57	−8.87	OD
Mean		37.9±6.40	8.38±2.02	27.60±1.53	−9.55±2.52	
HM-recent						
	F	17	2y	26.46	−8.25	OD
	F	18	2y	26.36	−6.25	OD
	M	19	4y	26.40	−6.5	OS
	M	19	3y	28.63	−8.25	OD
	F	18	2y	27.18	−8.0	OS
	M	21	4y	31.05	−11.5	OD
	M	22	4y	28.09	−9.75	OD
	F	24	3y	28.57	−9.75	OS
	F	24	3y	27.03	−7.5	OD
	F	24	2y	27.08	−7.25	OS
	F	25	4y	26.88	−6.5	OS
	M	21	2y	27.05	−6.75	OS
	M	21	2y	27.43	−7.0	OD
Mean		21.0±2.68	2.84±0.90	27.55±1.29	−7.94±1.57	
P		0.000	0.000	0.93	0.063	

HM-recent: the aqueous humor of young patients with high myopia; HM-long-term: the aqueous humor of older patients with high myopia; F: female; M: male; OD: right eye; OS: left eye.

DIA data were analyzed with SpectronautTM 14.4.200727.47784, searching the above constructed spectral library. The main software parameters were set as follows: retention time prediction type is dynamic iRT, interference on MS2 level correction is enabled, and cross-run normalization is enabled. All results were filtered based on a Q value cutoff of 0.01 (equivalent to FDR<1%).

Bioinformatic analysis: Cluster 3.0 and Java Treeview software were used to perform hierarchical clustering analysis. CELLO, which is a multiclass support vector machine (SVM) classification system, was used to predict protein subcellular localization [12,13]. Protein sequences were searched using the InterProScan software to identify protein domain signatures from the InterPro member database Pfam [14]. The gene ontology (GO) [15] and KEGG [16] pathway enrichment analysis was processed through cluster Profler an R package. The adjusted p- and q-values were both <0.05. Enrichment analysis was applied based on Fisher's exact test, by considering the whole quantified proteins as a background data set. The protein–protein interaction (PPI) information was

retrieved from IntAct molecular interaction database () by their gene symbols or STRING software and visualized with Cytoscape software version 3.2.1.

The WGCNA algorithm, which is another method of bioinformatics analysis, is a common algorithm for constructing weighted coexpression networks. This experiment used the R package WGCNA (R Version 3.4) to write a script to build a weighted coexpression network.

ELISA and receiver operating characteristic (ROC) curve analysis: Three proteins (PLG, KNG-1, and Alpha-1-antitrypsin) were chosen for verifying the differential expressions using ELISA. The Human Plasminogen ELISA kit (Elabscience Biotechnology Co., Ltd., E-EL-H2102c), Human KNG-1 kit (Cloud-Clone Co., Ltd., 7692281E3D), and Human Alpha-1-antitrypsin kit (Abcam, ab108799) were used. ELISA assays were performed according to the manufacturer's protocols, and samples (HM-long-term group, 13 samples; HM-recent group, 13 samples) were run in duplicate. The absorbances of the standards and samples were determined by spectrophotometry at 450 nm with a microplate reader. Statistical analyses were performed with GraphPad Prism version 6.0. The Student *t* test was applied for comparisons of quantitative data, and the ROC curve analysis with GraphPad Prism version 6.0 was performed to evaluate the sensitivity and specificity of the proteins.

RESULTS

Thirty-eight differentially expressed proteins (DEPs) were identified and quantitatively analyzed: The spectral library that was generated—as described in the experimental methods—contained 4,256 peptides corresponding to 1,146 protein groups. Then, the individual sample was subjected to DIA experiments to identify the aqueous humor proteins. As a result, a total of 4,353 peptides corresponding to 464 proteins were quantified (Appendix 1). Among proteins showing significant changes ($p<0.05$) in abundance, we used proteins with values of an abundance fold change >1.5 to identify those with a significant difference between the HM-long-term and HM-recent groups.

The study showed 38 DEPs, including 18 upregulated and 20 downregulated proteins (Figure 1A, Table 2). For these DEPs, we performed a series of analyses. First, we performed a hierarchical cluster analysis. The results showed that the DEPs can be distributed in different groups, indicating that the screening results can represent the impact of biologic processing on the samples (Figure 1B). Then, we performed a volcano plot of those DEPs. Consistently, the results showed that the DEPs were clearly distributed in different regions (Figure 1C). Here, to show the DEPs more intuitively, we performed box plot processing on the eight most upregulated DEPs (Figure 1D).

Functional analysis of DEPs:

Protein domains of DEPs are more extensive— Surprisingly, although 13 DEPs were located in the nucleus, we found nearly half of the proteins contained extracellular Appendix 2. In addition, the results showed that the domains of DEPs are more extensive, with seven proteins containing the immunoglobulin V-set domain (Appendix 2). Subsequently, we performed domain enrichment analysis on DEPs using Fisher's exact test to find the most significant enrichment domains and their corresponding DEPs (Appendix 2).

GO analysis reveals that DEPs have annotated nearly 1,000 functions—To understand the function, location, and biologic pathways of the protein in the organism thoroughly, we annotated the DEPs through GO analysis. The results showed that 38 DEPs were involved in 936 functional annotations (Figure 2). The most significant annotation functions were the positive regulation of catabolic process, regulation of catabolic process, positive regulation of cellular catabolic process for biologic process, steroid binding, and phospholipid binding.

KEGG analysis shows that complement and coagulation cascades are highly correlated with high myopia: First, we annotated the pathways of the top 20 DEPs. The results showed that two DEPs were involved in complement and coagulation cascades (Figure 3A,B). Next, we annotated and assigned metabolic pathways. The results showed that 21 DEPs participated in 11 metabolic pathways, including Transport and catabolism and Signal transduction (Figure 3C). Finally, we performed a KEGG pathway enrichment analysis on upregulated and downregulated DEPs. The affected pathways upregulated the proteins involved in the complement and coagulation cascades and proteoglycans in cancer and downregulated the proteins involved in lysosome, protein digestion, and absorption (Figure 3D).

Alpha-1-antitrypsin has the highest connectivity: PPIs were analyzed with the STRING database and classified according to DEP functions (information from GO, UniProt, and National Center for Biotechnology Information [NCBI]). These interacting proteins were divided into six categories that were mainly involved in the complement coagulation cascade, enzyme inhibitor activity, lipid metabolism, cell adhesion, and immune response. Appendix 3 presents the results.

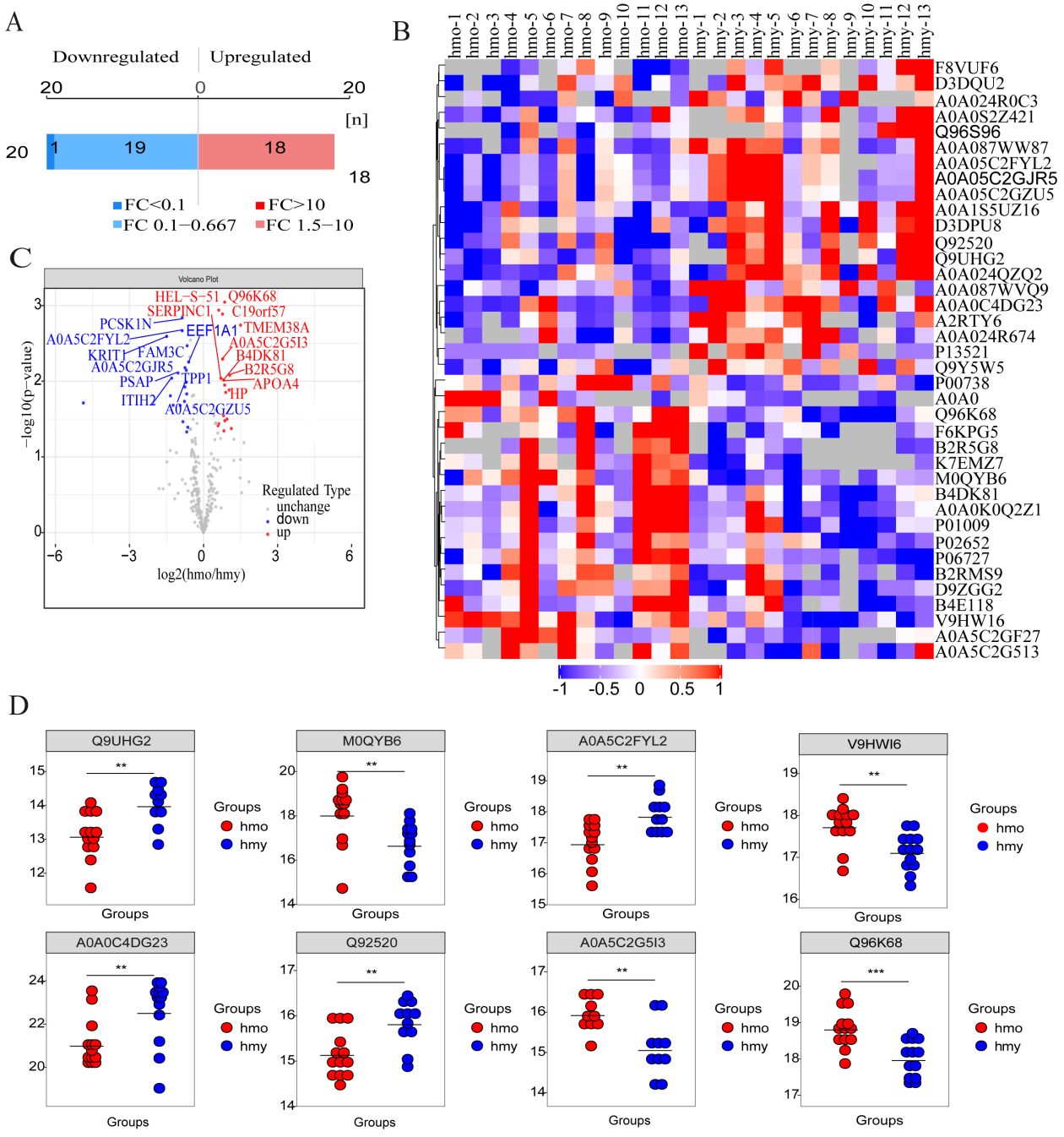

Figure 1. Presentation of DEPs. **A**: Number of DEPs. **B**: Hierarchical cluster analysis of the DEPs (Columns represent samples, rows represent proteins, and the shorter the distance of cluster branches, the higher the similarity of proteins). Red represents upregulated proteins, blue represents downregulated proteins, and gray represents no protein quantitative information. **C**: DEPs volcano plot showed that these were distributed in two different quadrants (the logarithm of the fold change of each quantifiable protein was taken as base 2, and the negative logarithm of the p value was taken as base 10). The horizontal axis represents the fold change (log2 value) of the differential protein, and the vertical axis represents the p value (-log10 value). Gray dots represent proteins with insignificant differences, red dots represent upregulated proteins, and blue dots represent downregulated proteins. The top 10 protein was selected to display. **D**: Box plot of 9 DEPs. *** p<0.001, ** 0.001<p<0.01, * 0.01<p<0.05.

Table 2. Quantitative proteomic analysis of 38 differentially expressed proteins, including 18 upregulated and 20 downregulated proteins.

Accession	Gene symbol	HM-long-term/ HM-recent	Description	P value
Downregulated proteins				
Q9UHG2	PCSK1N	0.55	ProSAAS	0.0015
A0A5C2FYL2		0.55	IGL c2002_light_IGKV1–39_IGKJ1 (Fragment)	0.0022
A0A0C4DG23	KRIT1	0.35	Krev interaction trapped protein 1 (Fragment)	0.0026
Q92520	FAM3C	0.63	Protein FAM3C	0.0034
A0A087WVQ9	EEF1A1	0.66	Elongation factor 1-alpha 1	0.0056
A0A5C2GJR5		0.59	IG c837_light_IGKV1–39_IGKJ2 (Fragment)	0.0066
D3DQU2	TPP1	0.62	Tripeptidyl peptidase I, isoform CRA_a	0.0072
A0A024QZQ2	PSAP	0.49	Prosaposin,isoform CRA_b	0.0078
A2RTY6	ITIH2	0.41	Inter-alpha (Globulin) inhibitor H2	0.0091
A0A5C2GZU5		0.62	IG c1300_light_IGKV1–12_IGKJ1 (Fragment)	0.0103
A0A1S5UZ16	ABI3BP	0.59	Target of Nesh-SH3	0.0119
F8VUF6	DCN	0.62	Decorin (Fragment)	0.0147
A0A087WW87	IGKV2–40	0.39	Immunoglobulin kappa variable 2–40	0.0156
D3DPU8	COL9A2	0.58	Collagen, type IX, alpha 2, isoform CRA_a	0.0185
P13521	SCG2	0.03	Secretogranin-2	0.0193
A0A024R674	SPTB	0.43	Spectrin beta chain	0.0207
Q9Y5W5	WIF1	0.52	Wnt inhibitory factor 1	0.0209
A0A0S2Z421	MYOC	0.56	Myocilin trabecular meshwork inducible glucocorticoid response isoform 1 (Fragment)	0.0342
Q96S96	PEBP4	0.64	Phosphatidylethanolamine-binding protein 4	0.0405
A0A024R0C3	NNT	0.62	Nicotinamide nucleotide transhydrogenase, isoform CRA_a	0.0467
Upregulated proteins				
Q96K68		1.82	cDNA FLJ14473 fis	0.00090
V9HWI6	HEL-S-51	1.53	Epididymis secretory protein Li 51	0.0012
K7EMZ7	C19orf57	1.70	Uncharacterized protein C19orf57	0.0013
M0QYB6	TMEM38A	2.82	Trimeric intracellular cation channel type A	0.0018
A0A5C2G5I3	AFM	1.71	IGL c3115_light_IGLV7–46_IGLJ1 (Fragment)	0.0051
B2R5G8		2.08	Serum amyloid A protein	0.0084
B4DK81		1.63	cDNA FLJ60621	0.0092
A0A0K0Q2Z1	SERPINC1	1.76	Serpin peptidase inhibitor clade C member 1	0.0096
P06727	APOA4	1.81	Apolipoprotein A-IV	0.0112
P00738	HP	2.05	Haptoglobin	0.0131
F6KPG5		1.86	Albumin (Fragment)	0.0141
P02652	APOA2	1.75	Apolipoprotein A-II	0.0284
A0A5C2GF27		1.93	IG c97_heavy_IGHV3–7_IGHD1–7_IGHJ1 (Fragment)	0.0316
B2RMS9	ITIH4	1.82	Inter-alpha (Globulin) inhibitor H4	0.0333
B4E1I8		1.53	cDNA FLJ54228	0.0364
P01009	SERPINA1	1.50	Alpha-1-antitrypsin	0.0386
A0A0G2JIW1	HSPA1B	2.18	Heat shock 70 kDa protein 1B	0.0421
D9ZGG2	VTN	1.77	Vitronectin	0.0453

Phenotype and omics association analysis:

Construction of coexpression modules for DEPs— WGCNA is a tool for examining the potential mechanisms of gene networks [17]. First, we constructed a protein coexpression module. The 426 proteins in 26 samples from 11 patients with HM-recent and nine patients with HM-long-term were used to construct the coexpression network. The results of the cluster analysis are shown in Appendix 3. Soft-threshold power was introduced into the network topology, which affected the scale independence and mean connectivity of the network. Following screening, a soft threshold of five was used to obtain the approximate scale-free topology with a scale-free topology ft index >0.9 and the lowest power (Appendix 3). As indicated in Appendix 3, three modules were identified in which proteins had similar coexpression traits.

The blue module is the key module—We used experimental groups as traits to analyze the interaction associations among these modules. The network heatmap of identified proteins indicated a relatively high level of independence among these clusters (Appendix 4). Focusing on the age trait (HM-recent and HM-long-term), the blue module exhibited the highest positive correlation (r=0.45; p=0.02) and highest negative correlation (r=-0.45; p=0.02; Appendix 4). Therefore, the blue module was identified as a key module for high myopia. Additional associations were then identified between

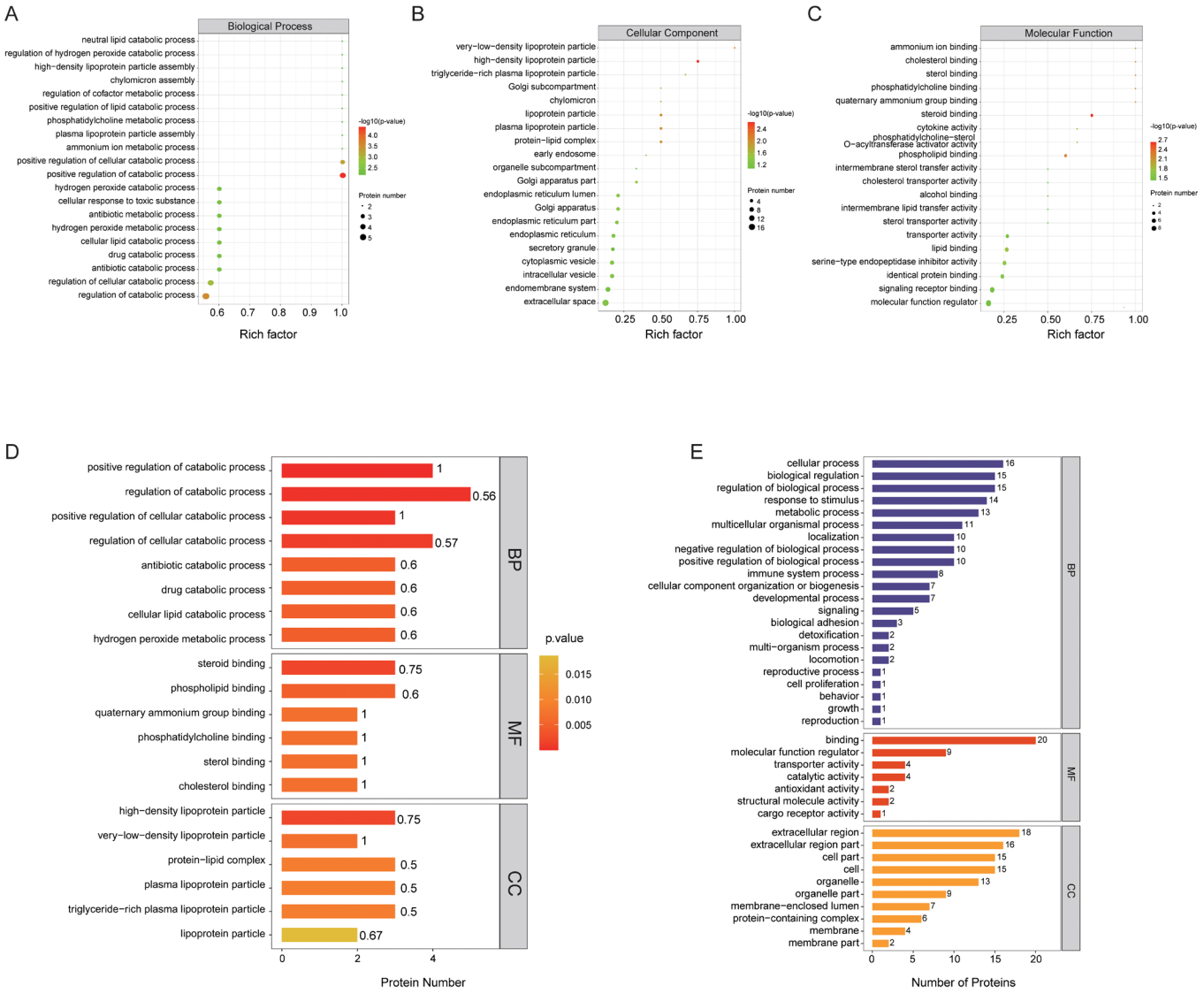

Figure 2. GO analysis of DEPs. (**A-C**) Major gene ontology terms were significantly enriched for the DEPs. **D**: Analyze the number of differential proteins on the GO secondary function annotation.

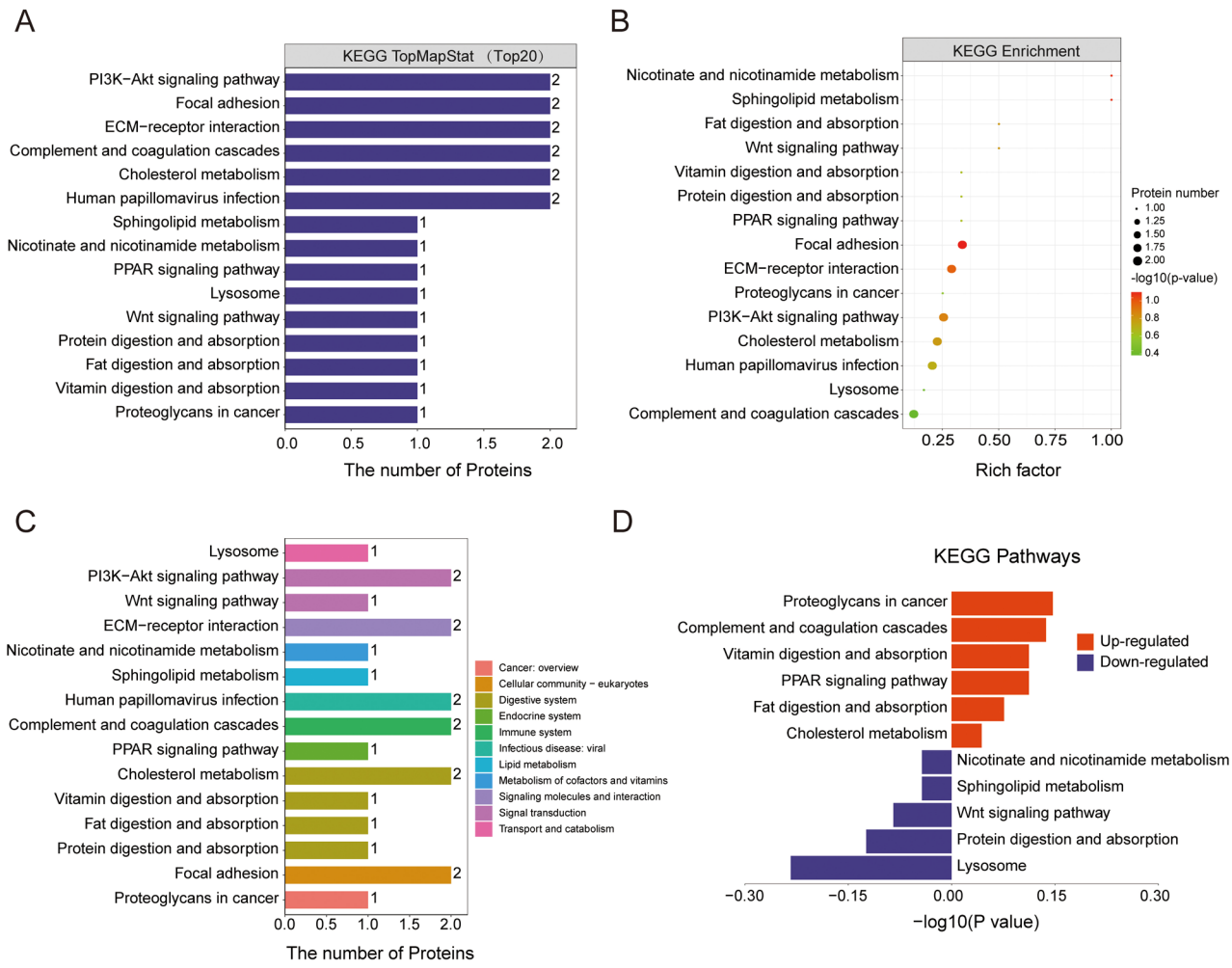

Figure 3. KEGG analysis of DEPs. **A, B:** Kyoto Encyclopedia of Genes and Genomes (KEGG) enrichment analysis of DEPs (select the top 10 by the value of p.adjust). **C**: Pathway metabolic pathway annotation of DEPs. Pearson correlation analysis of the proteins involved in the gene set enrichment analysis (GSEA) complement coagulation cascade. **D**: Pathway enrichment butterfly diagram for the upregulation and downregulation of DEPs.

module membership (MM) and protein significance (PS) for age. The significant correlations between blue MM and PS for HM-long-term and HM-recent are presented in Appendix 4. We observed the scattered distribution of protein significance (relativity between protein and trait/sample) and MM (relativity between protein and module) in each module to explore the correlation between protein and module in the key modules.

Functional enrichment analysis in modules of interest reveals that complement and coagulation cascade may be related to the pathogenesis of high myopia: GO and KEGG pathway enrichment analyses were performed on the blue protein clusters. The GO enrichment results demonstrated that blue module proteins were significantly associated with platelet al.pha granule, blood microparticle, and platelet degranulation (Figure 4A). The KEGG pathway enrichment results demonstrated that the proteins in the blue module were primarily enriched in complement and coagulation cascade (Figure 4B), which is in agreement with upregulated protein KEGG enrichment analysis.

Module visualization and identification of three hub genes: The intramodular connectivity was ranked according to the kME value, and all proteins of the blue module of interest were used to visualize the specific modules. Subsequently, the top three proteins of blue modules were labeled as the hub proteins (SUB1 regulator of transcription, serum amyloid A protein, and PLG) because they were most positively statistically relevant modules (Figure 4C). This result further confirms that the PLG protein may play an extremely

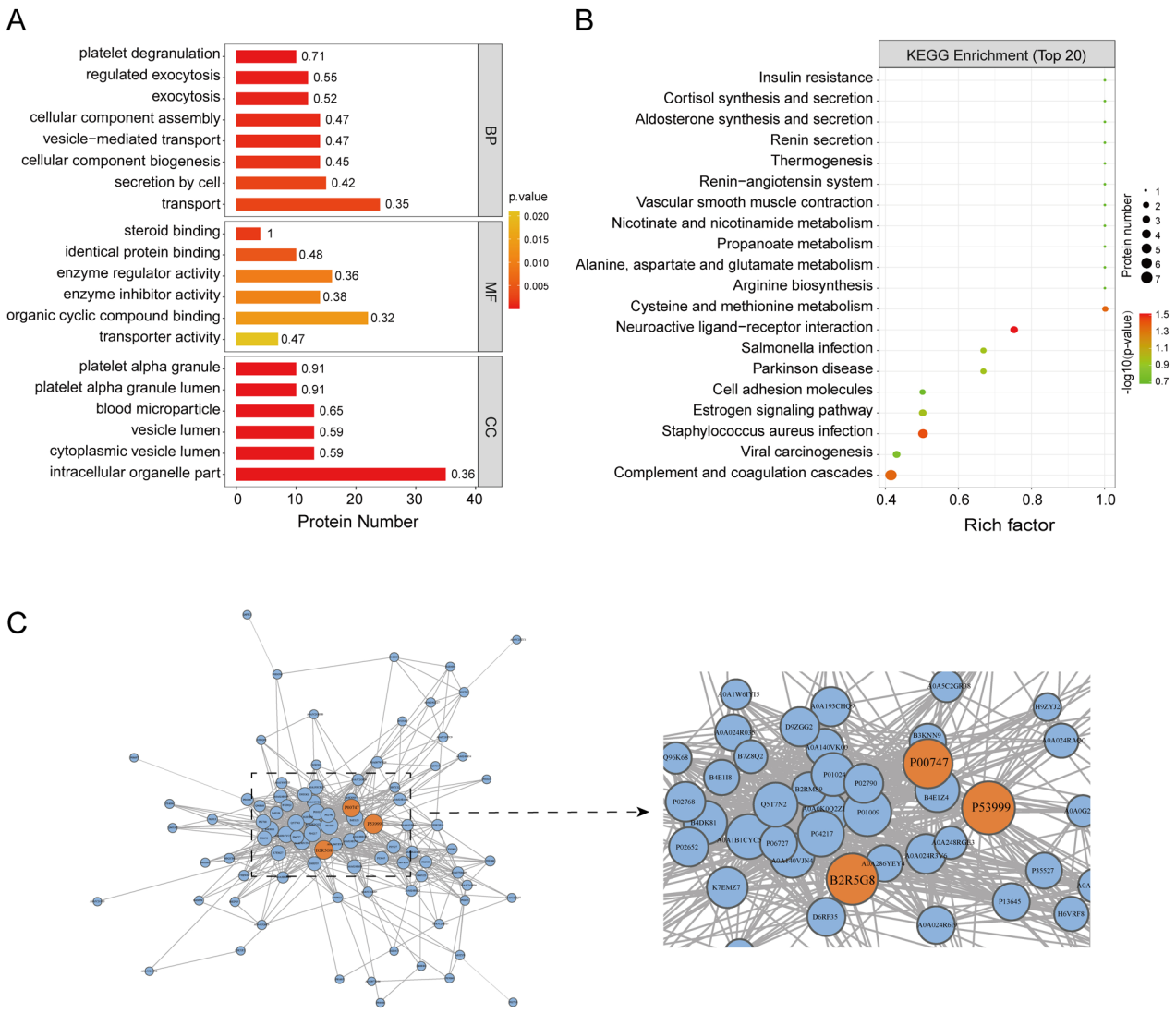

Figure 4. Functional enrichment analysis in modules of interest. **A**: GO enrichment of the blue modular. **B:** KEGG enrichment of the blue module. **C:** Coexpression network of protein in the blue module. SUB1 regulator of transcription, serum amyloid A protein, and PLG were labeled as the hub proteins.

important role in the pathogenesis of high myopia damage to the eye.

Validation with ELISA: We used the ELISA kit to verify the PLG protein, KNG-1 protein, and Alpha-1-antitrypsin protein expression in the aqueous humor of patients with HM-recent and HM-long-term. The expression levels of Alpha-1-antitrypsin were significantly upregulated in HM-long-term, while PLG and KNG-1 proteins were not statistically different between the two groups, which showed the same trend of change as the proteomic results (Figure 5A-C).

The areas under the ROC curves were calculated as measures of the specificity and sensitivity of the confirmed protein (Figure 5D-F). The accuracy of the area under the ROC curve was assessed as follows: 0.9–1=excellent; 0.8–0.9=good; 0.7–0.8=fair; and <0.7=not useful. The ROC analysis identified that Alpha-1-antitrypsin was informative (AUC: 0.8654, 95% confidence interval: 0.7052–1.026).

DISCUSSION

The advancement of surgical technology has provided valuable clinical samples for studying the pathogenesis of high myopia. Intraocular collamer lenses that can correct refractive errors without changing corneal morphology while retaining accommodation of the human eye [18,19]

have gradually become a mainstream refractive surgery. This makes it possible for us to obtain the aqueous humor of patients with high myopia of different ages. Although various studies, including genomics, transcriptomics, and proteomics, have been implicated to identify potential biomarkers (genes or proteins) for predicting high myopia and reveal the underlying mechanism, comprehensive proteomics research on the effect of age on the aqueous humor of high myopia is limited [3,8,9]. Here, we report a specific variant of DIA proteomic analysis of the protein changes in the aqueous humor of high myopia in two groups of patients of different ages. First, age had a certain effect on the type and content of aqueous humor protein in patients with high myopia, even though the number of DEPs identified was small. Second, we proved that, in the aqueous humor of highly myopic patients with no posterior scleral staphyloma, age had no effect on the expression of PLG protein and KNG-1 protein. Third, the upregulated DEPs were highly concentrated in the complement and coagulation cascade pathway, which is consistent with our previous research results, indicating that this pathway is closely related to the mechanism of high myopia causing damage to the eyeball. Therefore, we present a new model showing that there may be a time point below which the expression level of PLG protein remains unchanged but beyond which the expression level of PLG protein is significantly upregulated, hence leading to the development of posterior scleral staphyloma. It is worth noting that we believe that the time nodes may have individual differences. Overall, the results of the DIA proteomic analysis might offer new insights for elucidating the mechanism of high myopia.

High myopia is etiologically heterogeneous and tends to be genetic in origin in previous generations. However, with changes in educational models and educational parameters, the number of acquired high myopia has gradually increased in recent years [20]. Ian George Morgan et al. attributed the progression of myopia in children aged 6 or 7 to age-specific East Asian progression rates, predicting them to reach high myopia thresholds within 5 to 6 years [20]. However, whether continuous changes in the environment can cause or accelerate the occurrence of high myopia by acting on genes or proteins is unknown. Therefore, it is important to study the changes in the genes and proteins of high myopia at different ages. The present study is the first to investigate the effect of age on the level of aqueous humor protein in high myopia by using DIA proteomic analysis. The number of proteins (464) identified in the current study is roughly the same as that of previous studies, but the number of DEPs (38) is significantly reduced, which may be related to the younger age of the patients we recruited [8,21]. We used two methods of bioinformatics analysis, including conventional DEPs identification and searching for hub proteins related to high myopia and traits (age) through WGCNA, which enabled us to understand the pathogenesis of high myopia more thoroughly. Moreover, the PLG protein was identified as one hub protein, which is consistent with our previous research results [8] that

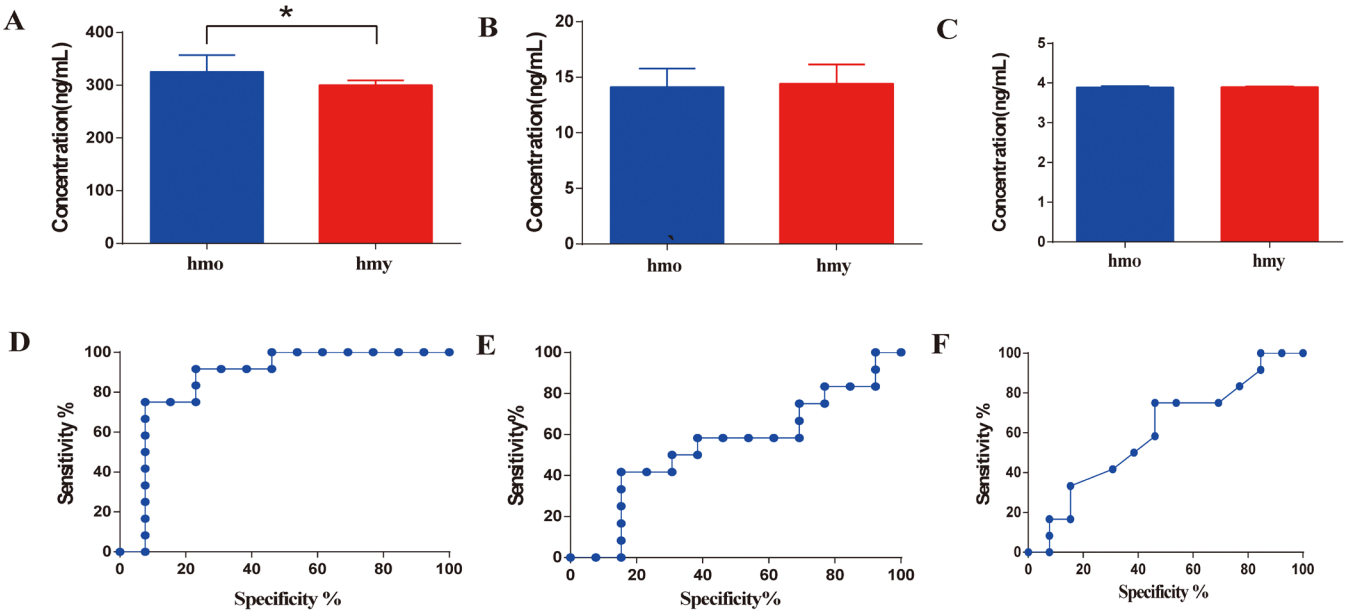

Figure 5. ELISA verification results. **A-C**: Result of Alpha-1-antitrypsin, KNG-1, and PLG of ELISA, respectively. **D-F**: Result of Alpha-1-antitrypsin, KNG-1, and PLG of ROC curve analysis for the specificity and sensitivity, respectively. *, p<0.05.

indicated that the PLG protein has a certain correlation with age. We discovered for the first time that the expression of the PLG protein in aqueous humor with high myopia may increase with age. Accordingly, our research results have the potential to help in exploring the time course of high myopia damage to the eyeball.

The mechanism by which high myopia develops into pathological myopia remains unclear. Pathological high myopia impairs the visual function of patients, mainly because of the occurrence of complications, including posterior staphyloma and various lesions of myopic maculopathy [22]. However, these complications occur in later life, so many young patients with a risk of developing myopic complications in the future are often overlooked. Posterior scleral staphyloma is an outpouching of a circumscribed posterior fundus region and has a curvature radius smaller than the curvature radius of the adjacent eye wall, which is the hallmark of the fundus of pathologic high myopia [23]. Therefore, it is important to identify the initiator of posterior scleral staphyloma. The remodeling of the extracellular matrix of the sclera is associated with a reduction in size of the individual collagen fibrils with a preponderance of unusually small diameter fibrils averaging below 60–70 nm [24]. The upregulated DEPs and the proteins in the green module of WGCNA in the present study were highly concentrated in the coagulation and complement cascades. The complement system might promote extracellular matrix (ECM) remodeling in the sclera, which has been confirmed by many studies [25,26]. Therefore, the coagulation and complement cascade may be an important initiating factor for high myopia complicated by posterior scleral staphyloma. This is consistent with our previous research results [8]. Moreover, there was no statistical difference in protein PLG in the present study because there were no complications among the patients with high myopia.

Our study had several limitations. First, the sample size was relatively small because of the stringent patient recruitment criteria. Second, the ages of the patients in the HM-long-term greatly varied, which may be one reason for the smaller number of DEPs. Third, although we have found the effect of age on aqueous humor in patients with high myopia, there has been no experimental verification at the cellular or animal levels. This will be the focus of our next work.

In conclusion, the findings from the present study of the aqueous humor of high myopia patients of different ages indicate that age had little effect on the protein in aqueous humor before high myopia complicated by posterior scleral staphyloma. In addition, the expression of the PLG protein may be related to age.

Ethics approval and consent to participate: The current study was approved by the Human Research Ethics Committee of Tianjin Medical University Eye Hospital and adhered to the tenets of the Helsinki Declaration of 1975, as revised in 2000 (5). Informed consent was obtained from all patients for inclusion in the present study.

APPENDIX 1. SUPPLEMENTAL FIGURE 1.

To access the data, click or select the words "Appendix 1." **A**: The number of peptides and proteins identified in hmo and hmy groups, respectively. **B**: Number of repetitive proteins identified in hmo and hmy groups. **C**: The result of principal component analysis (PCA), indicating that there were significant differences in protein expression between the hmo and hmy.

APPENDIX 2. SUPPLEMENTAL FIGURE 2.

To access the data, click or select the words "Appendix 2." **A**: Subcellular location distribution of DEPs. **B**: Domain analysis of DEPs (top 20). **C**: The results of domain enrichment analysis of DEPs using Fisher's exact test. The abscissa is the enrichment factor (Rich Fator≤1). The ordinate indicates the number of DEPs. The color of the bubble indicates the significance of the enriched domain classification (the P value is calculated based on the Fisher's Exact Test).

APPENDIX 3. SUPPLEMENTAL FIGURE 3.

To access the data, click or select the words "Appendix 3." **A**: PPI of DEPs. **B**: Cluster dendrogram. Each color represents one specifc co expression module, and branches above represent genes. **C**, **D**: Soft threshold selection process.

APPENDIX 4. SUPPLEMENTAL FIGURE 4.

To access the data, click or select the words "Appendix 4." **A**: Cluster dendrogram of all protein correlation within the module. The dark color indicates that the expression pattern between the proteins has a high degree of overlap. **B**: Heatmap of the correlation between clinical traits (age) and module. **C**, **D**: Correlation between MM of modules of interest and PS with clinical traits (age). **C**: Scatter plot of PS for hmo vs. MM in the blue module. **D**: Scatter plot of PS for hmy vs. MM in the blue module.

ACKNOWLEDGMENTS

Grant numbers: [Binhai New Area Health Commission 2023 science and technology project]under Grant [number 2023BWKQ019]. The authors thank Jing Sun, Shaozhen Zhao, Haorun Zhang, Yongtai Li for important clinical and

scientific suggestions. No conflicting relationship exists for any author. No honorarium, grant, or other forms of payment was given to anyone to produce the manuscript. Consent for publication: Each author listed on the manuscript has seen and approved the submission of this version of the manuscript and takes full responsibility for the manuscript. Competing interests: No potential conflict of interest was reported by the authors. Funding: This work was supported by the [Autonomous and open project of Tianjin Key Laboratory of Retinal Function and Diseases] under Grant [number 2020tjswmm002]; [Funded by Tianjin Key Medical Discipline (Specialty) Construction Project] under Grant [number TJYXZDXK-037A]; [Tianjin Education Commission Scientific Research Project (Natural Science)] under Grant [number 2022ZD059]; [Tianjin Science and Technology Plan Project (subject)] under Grant [number 21KPHDRC00140]; [Tianjin Medical University Eye Hospital High-level Innovative Talent Programme] under Grant [number YDYYRCXM-E2023–04]. Author contributions: Data curation, Kai Wen, Mengjun Fu, Haorun Zhang, Jingli Liang, Yang Cai, Yaoling Li, Ruihong Su, Yifang Huang, Ming Liu and Yufeng Zhang; Formal analysis, Kai Wen, Jingli Liang and Xiu Wang; Funding acquisition, Jing Sun Jingli Liang; Project administration, Jing Sun; Validation, Yongtao Li; Writing – original draft, Kai Wen; Writing – review & editing, Shaozhen Zhao and Jing Sun. Availability of data and materials: The data sets generated during and analyzed during the current study are not publicly available due to we are conducting further research but are available from the corresponding author on reasonable request. Dr. Jing (TMUeye@163.com) and Dr. Zhao (zhaosz1997@sina.com) are co-corresponding authors for this paper.

REFERENCES

1. Holden BA, Fricke TR, Wilson DA, Jong M, Naidoo KS, Sankaridurg P, Wong TY, Naduvilath TJ, Resnikoff S. Global Prevalence of Myopia and High Myopia and Temporal Trends from 2000 through 2050. Ophthalmology 2016; 123:1036-42. [PMID: 26875007].

2. Mérida S, Villar VM, Navea A, Desco C, Sancho-Tello M, Peris C, Bosch-Morell F. Imbalance Between Oxidative Stress and Growth Factors in Human High Myopia. Front Physiol 2020; 11:463-[PMID: 32477165].

3. Kim EB, Kim HK, Hyon JY, Wee WR, Shin YJ. Oxidative Stress Levels in Aqueous Humor from High Myopic Patients. Korean J Ophthalmol 2016; 30:172-9. [PMID: 27247516].

4. Markesbery WR, Lovell MA. Damage to lipids, proteins, DNA, and RNA in mild cognitive impairment. Arch Neurol 2007; 64:954-6. [PMID: 17620484].

5. Ito K, Suda T. Metabolic requirements for the maintenance of self-renewing stem cells. Nat Rev Mol Cell Biol 2014; 15:243-56. [PMID: 24651542].

6. Freddo TF. A contemporary concept of the blood-aqueous barrier. Prog Retin Eye Res 2013; 32:181-95. [PMID: 23128417].

7. Janero DR. Malondialdehyde and thiobarbituric acid-reactivity as diagnostic indices of lipid peroxidation and peroxidative tissue injury. Free Radic Biol Med 1990; 9:515-40. [PMID: 2079232].

8. Wen K, Shao X, Li Y, Li Y, Li Y, Wang Q, Su R, Zhang L, Cai Y, Sun J, Zhang Y. The plasminogen protein is associated with high myopia as revealed by the iTRAQ-based proteomic analysis of the aqueous humor. Sci Rep 2021; 11:8789-[PMID: 33888814].

9. Wen K, Zhang Y, Li Y, Wang Q, Sun J. Comprehensive analysis of transcriptome-wide m(6)A methylome in the anterior capsule of the lens of high myopia patients. Epigenetics 2020; •••:1-14. [PMID: 33108260].

10. Wiśniewski JR, Zougman A, Nagaraj N, Mann M. Universal sample preparation method for proteome analysis. Nat Methods 2009; 6:359-62. [PMID: 19377485].

11. Zhang F, Pu J, Gu Z, Mao H. DIA proteomics reveals hypotensive and immune-enhancing constituents in buffalo whey from different altitudes. Int J Biol Macromol 2020; 164:4146-54. [PMID: 32882282].

12. Yu CS, Lin CJ, Hwang JK. Predicting subcellular localization of proteins for Gram-negative bacteria by support vector machines based on n-peptide compositions. Protein Sci 2004; 13:1402-6. [PMID: 15096640].

13. Yu CS, Chen YC, Lu CH, Hwang JK. Prediction of protein subcellular localization. Proteins 2006; 64:643-51. [PMID: 16752418].

14. Zdobnov EM, Apweiler R. InterProScan–an integration platform for the signature-recognition methods in InterPro. Bioinformatics 2001; 17:847-8. [PMID: 11590104].

15. Götz S, García-Gómez JM, Terol J, Williams TD, Nagaraj SH, Nueda MJ, Robles M, Talón M, Dopazo J, Conesa A. High-throughput functional annotation and data mining with the Blast2GO suite. Nucleic Acids Res 2008; 36:3420-35. [PMID: 18445632].

16. Kanehisa M, Goto S, Sato Y, Furumichi M, Tanabe M. KEGG for integration and interpretation of large-scale molecular data sets. Nucleic Acids Res 2012; 40:D109-14. [PMID: 22080510].

17. Zhang B, Horvath S. A general framework for weighted gene co-expression network analysis. Stat Appl Genet Mol Biol 2005; 4:17-.

18. Zhu QJ, Wang MY, Yu P, Liang XS, Ma L, Xiao HX, Yuan Y. Analysis of macular microvasculature and thickness after ICL implantation in patients with myopia using optical coherence tomography. Int J Ophthalmol 2020; 13:1948-54. [PMID: 33344195].

19. Miao H, Chen X, Tian M, Chen Y, Wang X, Zhou X. Refractive outcomes and optical quality after implantation of posterior chamber phakic implantable collamer lens with a central hole (ICL V4c). BMC Ophthalmol 2018; 18:141-[PMID: 29898694].

20. Rose KA, French AN, Morgan IG. Environmental Factors and Myopia: Paradoxes and Prospects for Prevention. Asia Pac J Ophthalmol (Phila) 2016; 5:403-10. [PMID: 27898443].

21. Xiang M, Zhang X, Li Q, Wang H, Zhang Z, Han Z, Ke M, Chen X. Identification of proteins in the aqueous humor associated with cataract development using iTRAQ methodology. Mol Med Rep 2017; 15:3111-20. [PMID: 28339073].

22. Ohno-Matsui K. What Is the Fundamental Nature of Pathologic Myopia? Retina 2017; 37:1043-8. [PMID: 27755375].

23. Ohno-Matsui K, Jonas JB. Posterior staphyloma in pathologic myopia. Prog Retin Eye Res 2019; 70:99-109. [PMID: 30537538].

24. Curtin JB. The myopias, basic science and clinical management. Optom Vis Sci 1985; 64:76-.

25. Riddell N, Crewther SG. Novel evidence for complement system activation in chick myopia and hyperopia models: a meta-analysis of transcriptome datasets. Sci Rep 2017; 7:9719-[PMID: 28852117].

26. Gao TT, Long Q, Yang X. Complement factors C1q, C3 and C5b-9 in the posterior sclera of guinea pigs with negative lens-defocused myopia. Int J Ophthalmol 2015; 8:675-80. [PMID: 26309860].

Articles are provided courtesy of Emory University and the Zhongshan Ophthalmic Center, Sun Yat-sen University, P.R. China. The print version of this article was created on 20 March 2024. This reflects all typographical corrections and errata to the article through that date. Details of any changes may be found in the online version of the article.